Available online at www.sciencedirect.com
ScienceDirect
Trans. Nonferrous Met. Soc. China 26(2016) 649−657
Transactions of Nonferrous Metals Society of China
www.tnmsc.cn

Flow behavior and microstructure evolution of 6A82 aluminium alloy with high copper content during hot compression deformation at elevated temperatures

Qun-ying YANG, Dong YANG, Zhi-qing ZHANG, Ling-fei CAO, Xiao-dong WU, Guang-jie HUANG, Qing LIU
College of Materials Science and Engineering, Chongqing University, Chongqing 400045, China

Received 30 April 2015; accepted 10 November 2015

Abstract: The flow behavior and microstructure evolution of 6A82 aluminum alloy (Al−Mg−Si−Cu) with high copper content were studied on a Gleeble−1500 system by isothermal hot compression test in the temperature range from 320 to 530 ℃ and the strain rate range from 0.001 to 10 s^{-1}. The results reveal that the flow stress of the alloy exhibits a continuous flow softening behavior at low temperatures of 320−390 ℃, whereas it reaches steady state at high temperatures (≥460 ℃), which are influenced greatly by the Zener−Hollomon parameter (*Z*) in the hyperbolic sine with the hot deformation activation energy of 325.12 kJ/mol. Microstructure characterizations show that prominent dynamic recrystallization and coarsening of dynamic precipitation may be responsible for the continuous flow softening behavior. Due to deformation heating at high strain rates (≥1 s^{-1}), dynamic recrystallization is more prominent in the specimen deformed at 530 ℃ and 10 s^{-1} than in the specimen deformed at 460 ℃ and 0.1 s^{-1} even though they have very close ln *Z* values.

Key words: Al−Mg−Si−Cu aluminum alloy; isothermal hot compression; flow stress; dynamic recrystallization; dynamic precipitation

1 Introduction

Considerable commercial interest has been shown in Al−Mg−Si alloys [1], which are aging hardenable aluminum alloys and widely used in the automotive industry for structural parts due to their high specific strength and bending stiffness. Since most aluminum parts were used in the form of wrought products, high temperature formability of their alloys has been extensively studied for decades [2,3]. Precipitation hardening is the main strengthening mechanism in these alloys. Increasing the Cu content enhanced the strength but deteriorated their hot workability in 6xxx alloys. Therefore, the investigation of high temperature deformation behavior and the associated microstructure evolution would help to clarify the workability of these alloys.

Due to the high stacking fault energy of aluminum alloys, dynamic recovery (DRV) was more likely to occur than dynamic recrystallization (DRX) [4]. Many reports about high temperature deformation behavior and dynamic softening mechanisms of aluminum alloys have been published [5−7]. The previous investigations pointed out that the softening mechanisms and microstructure evolution are related to deformation temperature and strain rate, which are represented by the Zener−Hollomon parameter (*Z*). Recent studies on Al−Mg−Li−Zr alloy and Al−Zn−Mg−0.25Sc−Zr alloy have attributed the transformation of recrystallization mechanism to the change of deformation condition [8,9]. LIU et al [10] investigated the hot deformation behavior of AA7085 aluminum alloy and believed that dynamic recrystallization was more sensitive to deformation temperature than to strain rate. Although many researchers tried to explain the hot deformation behavior of aluminum alloy by different mechanisms, there was no perfect theory for the restoration behavior of aluminum alloys during hot deformation under different conditions. Thus, it is necessary to study the deformation behavior and microstructure evolution for aluminum alloys.

The occurrence of DRX and the measurement of recrystallized grain size were confirmed by optical

Foundation item: Project (2014DFA51270) supported by the International Science and Technology Cooperation Program of China; Project (CDJRC10130008) supported by the Fundamental Research Funds for the Central Universities, China; Project (51421001) supported by the National Natural Science Foundation of China
Corresponding author: Zhi-qing ZHANG; Tel: +86-23-65102016; E-mail: zqzhang@cqu.edu.cn
DOI: 10.1016/S1003-6326(16)64154-7

microscopy (OM) in previous studies. Recently, electron backscatter diffraction (EBSD) technique has been widely used in microstructure characterization [11−13]. EBSD can give more fundamental and accurate information about deformed and recrystallized grains, such as misorientation angle distribution, recrystallized grain size and texture component. The recrystallized grain size was quantitatively measured and the occurrence of DRX was observed by the EBSD technique in the present study.

In this work, a new Al−Mg−Si−Cu alloy based on 6082 alloy was used. The effects of the deformation conditions on the flow behavior and microstructure evolution of the high Cu aluminum alloy during compression deformation at elevated temperatures were studied. The aim of the present work is to gain a fundamental understanding of the hot deformation behavior of the new Al−Mg−Si−Cu aluminum alloy, which will provide a guide for optimizing the actual plastic deformation parameters.

2 Experimental

A new Al−Mg−Si−Cu alloy based on 6082 alloy (6A82) was applied in the form of the ingot. The compositions of the 6A82 alloy and 6082 alloy are shown in Table 1. Compared with 6082 alloy, the content of Cu increases and the content of Fe decreases in the 6A82 alloy. Cylindrical specimens of *d*8 mm × 12 mm were machined from ingot plate and subjected to a homogenization at 540 °C for 6 h in an air furnace, followed by water quenching. The microstructure of the homogenized specimen is shown in Fig. 1. It can be seen that the original grain size is about 60 μm with an average misorientation angle of 38.7°.

Table 1 Compositions of 6A82 and 6082 alloys (mass fraction, %)

Alloy	Mg	Si	Cu	Cr	Fe
6A82	0.89	1.02	0.46	0.15	0.12
6082	0.6−1.2	0.7−1.3	≤0.1	≤0.25	≤0.5
Alloy	Mn	Ni	Zn	Ti	Al
6A82	0.5	0.01	0.02	0.05	Bal.
6082	0.4−1.0	0.00	≤0.20	≤0.10	Bal.

The isothermal compression tests were carried out on a Gleeble−1500 thermal simulator at strain rates of 0.001−10 s^{-1} and deformation temperatures of 320−530 °C. In order to reduce friction and inhomogeneous deformation of the specimens, the flat ends of the specimens were coated with lubricant. The specimens were heated to the test temperature at a heating rate of 5 °C/s and held for 3 min prior to compression. As soon as the specimens were compressed to a final strain of 1.2, the specimens were quenched in water and then sectioned parallel to the compression axis.

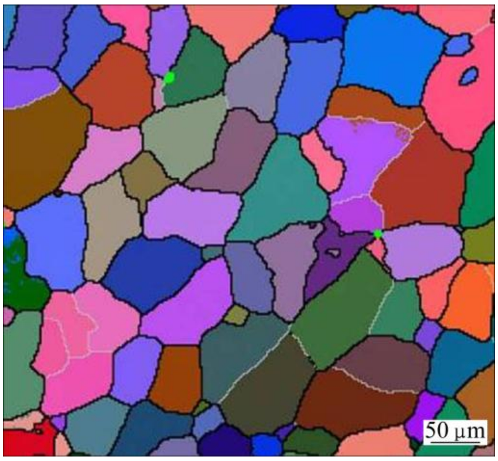

Fig. 1 Orientation map of 6A82 alloy after homogenization

The microstructures were characterized by optical microscopy (OM), electron backscatter diffraction (EBSD) and transmission electron microscopy (TEM) techniques. The specimens for metallographic observation were prepared by grinding, mechanical polishing and etching with the Keller’s reagent (2.5 mL HNO_3, 1.5 mL HCl, 1 mL HF and 95 mL H_2O). The specimens for EBSD measurement were electro-polished in a solution of 10% $HClO_4$ and 90% C_2H_5OH at −20 °C. The EBSD studies were carried out on a field emission gun-environmental scanning electron microscopy (FEG−SEM) FEI, at 20 kV and spot size number of 7. Thin foils of TEM specimens were prepared by cutting longitudinal sections of the deformed specimens using an electro-polishing unit operated at 10 V and −25 °C using 30% HNO_3 and 70% CH_3OH solution. TEM investigations were performed on a Zeiss Libra 200 FE transmission electron microscope operated at 200 kV.

3 Results and discussion

3.1 Flow stress behavior of 6A82 alloy

Figure 2 shows the true stress−true strain curves during hot compression under various deformation conditions. It can be seen that the flow stress increases with increasing strain rate and decreasing temperature. Moreover, the flow curves exhibit different shapes. At low temperatures (≤390 °C), the flow stress decreases monotonically after the peak stress till the final strain. At high temperatures (≥460 °C), the flow curves after the peak strain do not change obviously and the stable state is obtained at high strains.

Deformation at elevated temperatures is a competing process of the work hardening and dynamic

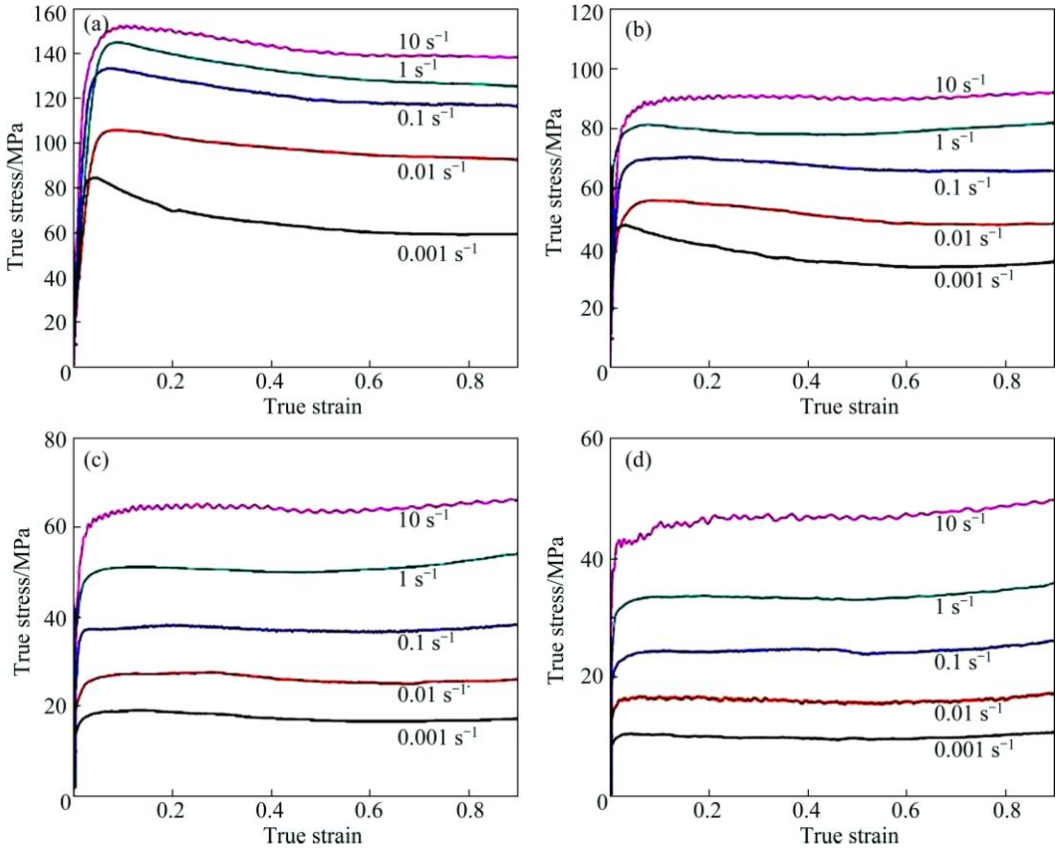

Fig. 2 True stress−true strain curves of 6A82 aluminum alloy during hot compression at different temperatures: (a) 320 ℃; (b) 390 ℃; (c) 460 ℃; (d) 530 ℃

softening. At the early stage of deformation, dislocation density increases rapidly due to the interaction and multiplying of dislocations, which results in a rapid increase in the flow stress. After the peak stress, dynamic softening such as DRV or DRX, can offset or partially offset working hardening, leading to a decrease in flow stress. Flow softening is a common characteristic of many alloys deformed at elevated temperatures. It is related to the thermal softening and microstructural softening [14]. The thermal softening is ascribed to deformation heating, whereas the microstructural softening consists of dynamic recovery, dynamic recrystallization and the coarsening of dynamic precipitation [15−17]. In the present study, the dynamic softening seems to be more prominent for specimens at low deformed temperatures than the ones deformed at high temperatures (Figs. 2(a) and (b)). And the extent of softening is more significant at low strain rates ($\dot{\varepsilon}\leq 0.1$ s^{-1}). Due to the absence of deformation heating at low strain rates ($\dot{\varepsilon}<1$ s^{-1}), the flow softening may be related to the microstructural softening.

3.2 Kinetic analysis

During hot deformation of aluminum alloys, it is generally accepted that constitutive equation can model the hot deformation behavior of the alloy and is sensitive to strain rate ($\dot{\varepsilon}$) and temperature (T), and can be described by the Zener−Hollomon parameter Z [18−20]:

$$Z=\dot{\varepsilon}\exp\left(\frac{Q}{RT}\right)=A[\sinh(\alpha\sigma)]^n \tag{1}$$

where A, n and α are constants, Q is the hot deformation activation energy, R is the mole gas constant, T is the deformation temperature, and σ is the stress. The hot deformation activation energy of Al−Mg−Si−Cu alloy can be obtained and the value is 325.12 kJ/mol. More details are described in Ref. [21]. The ln Z values can be obtained, as shown in Table 2.

Table 2 ln Z values of specimens under various deformation conditions

Temperature/℃	ln Z				
	0.001 s^{-1}	0.01 s^{-1}	0.1 s^{-1}	1 s^{-1}	10 s^{-1}
320	59.0	61.3	63.6	65.9	68.2
390	52.1$^{1)}$	54.4	56.7	58.9	61.3
460	46.4$^{1)}$	48.7$^{1)}$	51.1$^{1)}$	53.3	55.7
530	41.8$^{1)}$	44.1$^{1)}$	46.4$^{1)}$	48.7$^{1)}$	51.0$^{1)}$

1) Probable occurrence of partial or full dynamic crystallization

The hot deformation activation energy Q is an important indicator for the hot workability of materials. The value of Q in this work is 325.12 kJ/mol, which is higher than that of the solution-treated 6082 alloy (269 kJ/mol) [22] and that reported for pre-aged or annealed 6060 alloy (205 kJ/mol) [23] and 6082 alloy (192.83 kJ/mol) [24]. The hot deformation activation energy of aluminum alloy is related to its initial microstructure, chemical compositions and heat treatment conditions.

It is well known that the addition of Cu to Al−Mg−Si alloys affects mechanical properties, resulting in different precipitation sequences. Generally, in alloys without Cu, the precipitation sequence [25] is: SSSS → Atomic clusters → GP zones → β''→ B', U1, U2, β'→ β, Si. However, Q' phase precipitates in various morphologies when Cu is added, and a new precipitation sequence is followed [26]: SSSS → Atomic clusters → GP zones →β'', L/S/C, QP, QC, → β', Q'→ Q. Hence, the addition of Cu benefits the precipitation of Q' phase. JIN et al [27] reported that the lath-shaped Q' phase ($Al_5Cu_2Mg_8Si_6$) was observed by three-dimensional atom probe and TEM due to the addition of 0.6% Cu in 6082 alloy. Cu-segregation at the Q' interface retards and delays the coarsening of Q' phase. Fine precipitates pin grain boundaries and impede the growth of recrystallized grains [28−30], which leads to a high flow resistance as well as a high activation energy. Thus, the high activation energy (Q) found in the present new Al−Mg−Si−Cu alloy can be attributed to high copper content.

The deformation activation energy is enormously affected by heat treatment conditions. Higher hot deformation activation energy has been found in solution-treated aluminum alloys [22]. Small amount of addition elements could have significant effects on the boundary migration. For aluminum alloys containing small amount of Cu, the boundary velocity at constant driving force is inversely proportional to the solute concentration. At high deformation temperatures, more alloying elements would diffuse into the matrix of the alloy with high Cu content than that with low Cu content. These solute atoms diffuse to a stationary dislocation and then retard the movement of the dislocation, which results in an increase in the flow stress. On the other hand, high Cu component can provide larger driving force for SSS atomic clusters and accelerate natural aging kinetics [31]. At low deformation temperatures, the majority of solutes are precipitated out of the Al matrix in the form of the second phase particles [18]. The presence of these particles results in a high precipitation strengthening effect in solution-treated alloys. It can be concluded that the 6xxx alloys with high Cu content have much higher peak flow stress than the alloys with low Cu content, and the hot deformation activation energy Q of Cu-rich alloys is higher than that of Cu-free alloys. In this work, the high Q value of the alloy may be related to the high Cu content held in solution by the long high temperature solution process.

3.3 Microstructure evolution

Table 2 shows ln$Z$ values of the specimens deformed under various deformation conditions. The microstructures of specimens with different ln Z values are shown in Fig. 3. In these figures, the black lines represent high-angle boundaries (misorientation larger than 15°) and the grey lines represent low-angle boundaries (misorientation 2°−15°). It can be seen that the microstructures of all deformed specimens consist of elongated grains and fine equiaxed grains, which are the typical features of partial recrystallization. The DRX grain size depends on the Zener−Hollomon parameter. A linear relation between recrystallized grain size (D_{rex}) and ln Z can be established:

$$D_{rex}=-0.346 \ln Z+20.07 \quad (2)$$

As shown in Fig. 4, the recrystallized grain size depends on the ln Z value. With decreasing ln Z value, the recrystallized grain size increases gradually. The reasons may be the following aspects: 1) at high deformation temperatures, recrystallized nuclei are activated easily by the motion of atoms and dislocations; and 2) low strain rate means more time for recrystallization, the growth of recrystallized nuclei occurs easily through the migration of high-angle grain boundaries. Therefore, a coarser recrystallized grain size is observed at low ln Z value.

From Fig. 3, it can be found that the extent of recrystallization initially decreases and then increases with decreasing ln Z value. The microstructure of the specimen with high ln Z value exhibits prominent recrystallization (Fig. 3(a)). At moderate ln Z value (Fig. 3(b)), fine recrystallized grains near original boundaries reduce obviously, whereas the high-angle boundary segments marked with white arrows are found within deformed grains. With decreasing ln Z value (Figs. 3(c) and (d)), original grain boundaries become straight and clear. New recrystallized grains marked with white circles are observed at triple junctions and boundaries, as shown in Fig. 3(d). The corresponding misorientation angle distributions for the specimens with different ln Z values after hot compression are shown in Fig. 5. With decreasing ln Z value, the average misorientation decreases form 28.5° to 15.7° initially and then increases to 29.1° and 28.9°. The corresponding frequencies of LABs are 36.2%, 68.1%, 33.2% and 32.6%, respectively. Such a feature implies a change in the restoration mechanism between low ln Z value and high ln Z value.

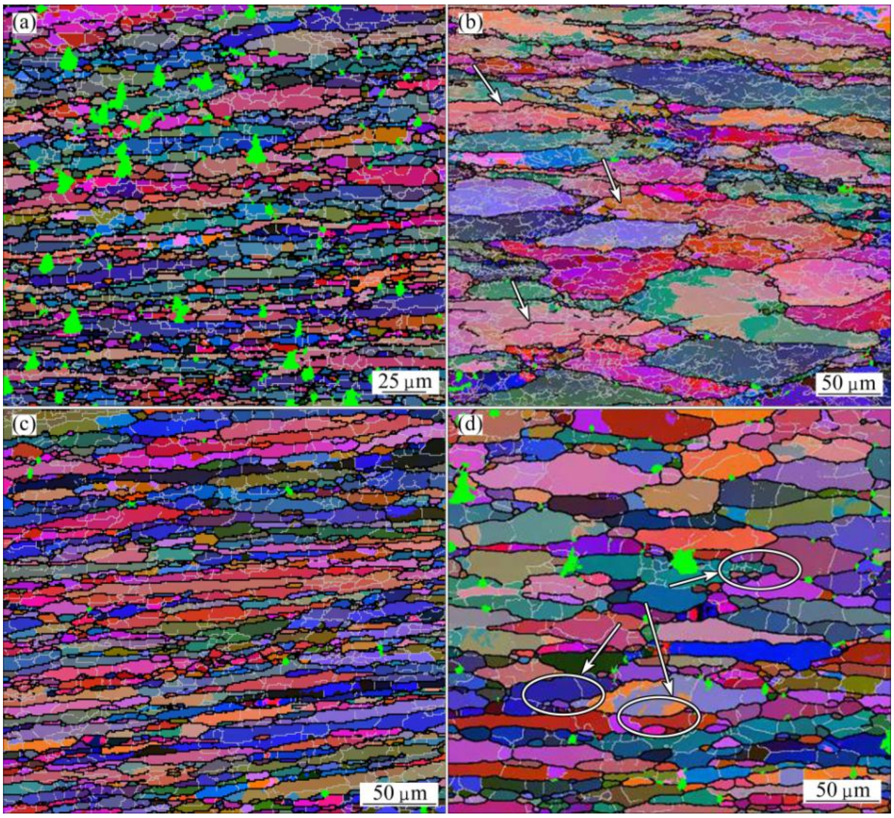

Fig. 3 All Euler maps of specimens after hot compression under different deformation conditions: (a) 320 °C, 0.001 s^{-1}, ln Z=59.0; (b) 460 °C, 1 s^{-1}, ln Z=53.3; (c) 530 °C, 0.01 s^{-1}, ln Z=44.1; (d) 530 °C, 0.001 s^{-1}, ln Z=41.8

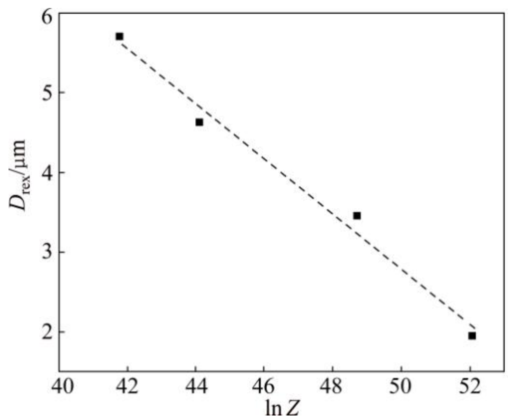

Fig. 4 Relationship between dynamic recrystallized grain size and ln Z value

Dynamic recovery and dynamic recrystallization are main restoration mechanisms during hot deformation in aluminum alloys. The changes of restoration mechanism under different conditions are reported in aluminum alloys [8,32,33]. The microstructure observation reveals that prominent recrystallization is observed at high ln Z value, illustrating that the softening mechanism is dynamic recovery and dynamic recrystallization. This observation suggests that low strain rate allows sub-grains to have sufficient time to merge or rotate and form gradually to new high-angle boundaries when the deformation temperature reaches the start temperature of recrystallization. As ln Z value decreases (Fig. 3(b)), the deformation time of the specimen with ln Z value of 53.3 is shorter than that of the specimen with ln Z value of 59.0. The transformation from low-angle boundary to high-angle boundary is restricted and the majority of the grains are still at a stage of recovery. With decreasing ln Z value (Figs. 3(c) and (d)), in the case of high-temperature deformation, the interaction between dislocations is more active than that of the low-temperature deformation, leading to an increase in annihilation and rearrangement of dislocation. In this case, the original grains are fragmented progressively by low-angle boundaries and finally form new free-strain region. Such a microstructure characteristic exhibits that ln Z value is not only an indicator to decide the occurrence of dynamic recrystallization.

It has been widely accepted that dynamic recrystallization only occurs at low Z values, which must be less than or equal to a critical value. Less attention has been paid to the microstructure difference of specimens with closer Z values. In order to reveal the microstructure differences of specimens with nearly identical ln Z values, the microstructures of specimens deformed at 460 °C, 0.1 s^{-1} and 530 °C, 10 s^{-1} are compared. The ln Z values of the two specimens are 51.1 and 51.0, respectively. The Euler maps and TEM images of the two specimens are shown in Fig. 6. The equiaxed grains, shown by white

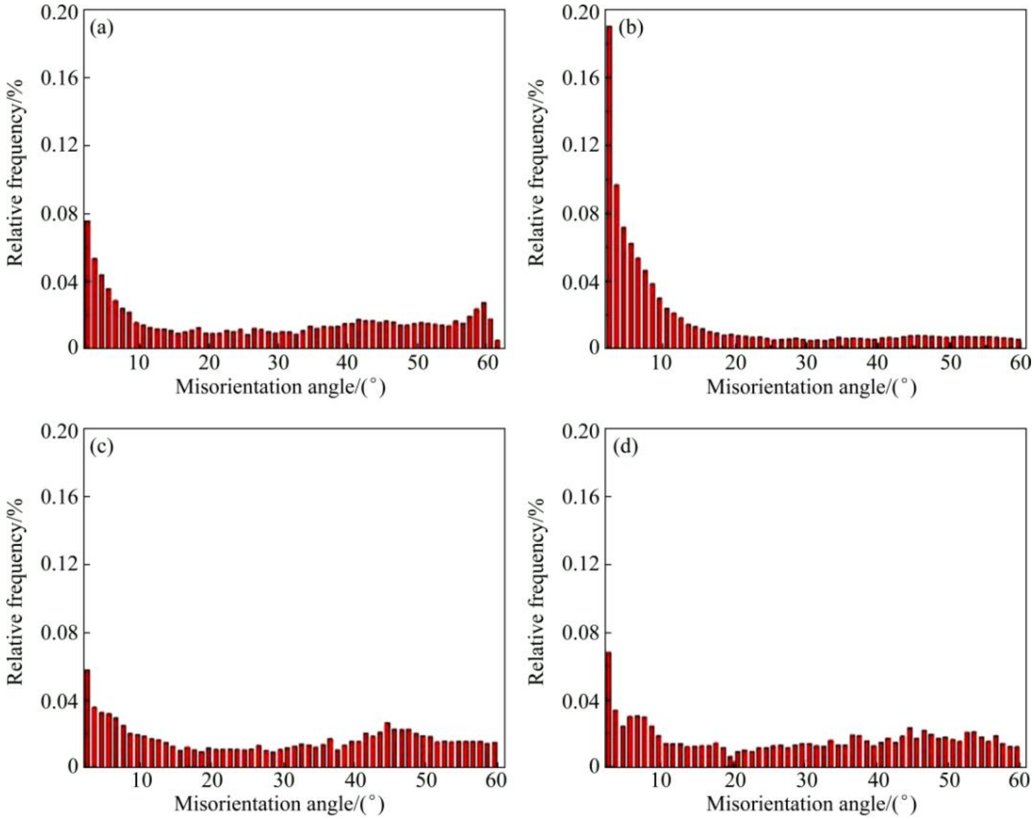

Fig. 5 Boundary misorientation angle distributions of hot deformed 6A82 aluminium alloy under different deformation conditions indicated by ln Z value: (a) ln Z=59.0, average misorientation of 28.5°; (b) ln Z=53.3, average misorientation of 15.7°; (c) ln Z=44.1, average misorientation of 29.1°; (d) ln Z=41.8, average misorientation of 28.9°

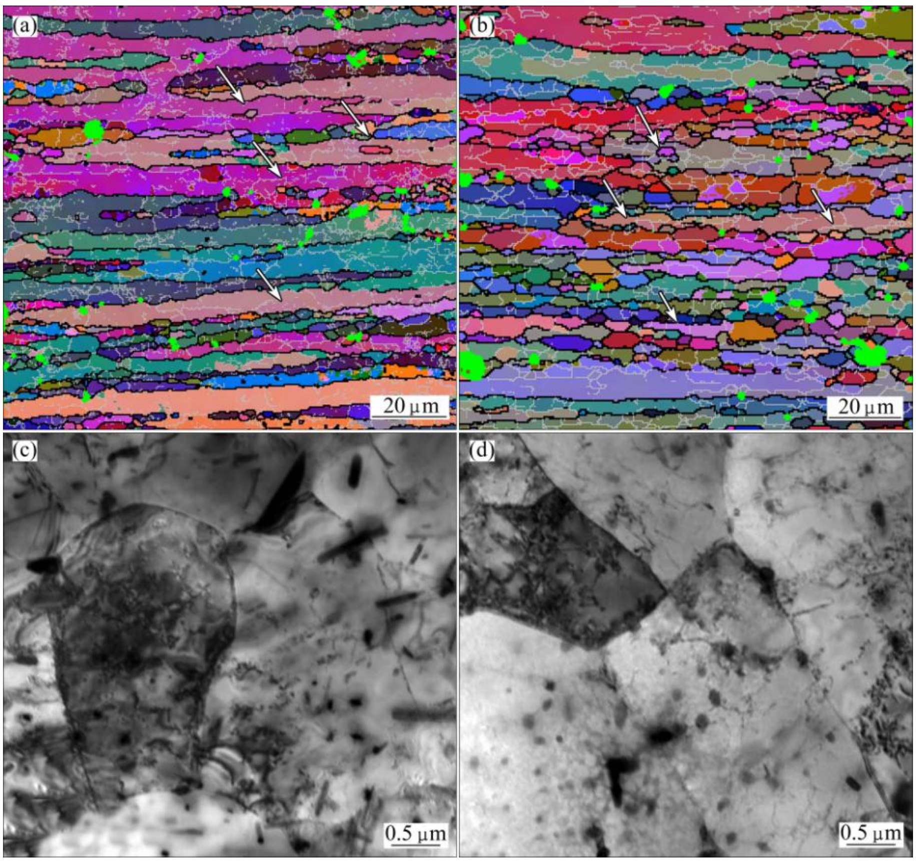

Fig. 6 Euler maps and TEM images of 6A82 aluminium alloy after hot compression under different deformation conditions: (a, c) 460 ℃, 0.1 s^{-1}, ln Z=51.1; (b, d) 530 ℃, 10 s^{-1}, ln Z=51.0

arrows in Figs. 6(a) and (b), clearly indicate that dynamic recrystallization occurs in these specimens. More prominent dynamic recrystallization is found in the specimen deformed at 530 ℃ and 10 s^{-1} than in the specimen deformed at 460 ℃ and 0.1 s^{-1}. This means that more prominent dynamic recrystallization is found in the specimen deformed at higher deformation temperature and strain rate (530 ℃, 10 s^{-1}) than in the specimen deformed at lower deformation temperature and strain rate (460 ℃, 0.1 s^{-1}). The reason may be ascribed to the following aspects. Firstly, at high temperatures, dislocations may be more easily climb or slide during compression. Sufficient migration of dislocations leads to the merging of some sub-grains and the transformation from low-angle boundaries to high-angle boundaries through absorbing dislocations. Then, the grain boundaries become straight and clear (Fig. 6(d)). Secondly, compared with the low deformation temperature (Fig. 6(c)), the second phase particles tend to dissolve at a high temperature of 530 ℃. The effect of the particles on pinning of grain boundaries is restricted. Consequently, the process of recrystallization is accelerated. Thirdly, the deformation heating increases with increasing strain rate. Energy generated by deformation heating cannot remove from the specimens, leading to an increase in actual temperature and the occurrence of dynamic recrystallization. The discrepancies between the actual temperature of deformed specimens and the pre-set temperatures were studied in Ref. [21]. It is found that the deformation heating can be ignored at low strain rates (≤0.1 s^{-1}). The temperature can be raised by nearly 30 ℃ (for example, at a strain rate of 10 s^{-1}). Based on the above analysis, dynamic recrystallization is more prominent in the specimen deformed at 530 ℃ and 10 s^{-1} than in the specimen deformed at 460 ℃ and 0.1 s^{-1}.

TEM images of the specimens deformed under various conditions are shown in Fig. 7. It can be seen that well-developed sub-grains and lamellar precipitates are visible after deformation at 320 ℃ and 0.01 s^{-1}. Small precipitates with a mean length of 0.3 μm distributed at the grain boundaries marked with white arrows (Fig. 7(a)) can effectively pin the low-angle boundary and inhibit dynamic recovery. With decreasing ln Z value (320 ℃, 0.001 s^{-1}), the majority of the particles become coarser, as shown in Fig. 7(b). The lamellar-like particles have mean length and width of 0.9 and 0.2 μm, respectively. The microstructure observation illustrates that the continuous flow softening is related to the coarsening of dynamic precipitation. LIU et al [18] considered that further deformation after the peak strain can actually promote the coarsening of these particles although there

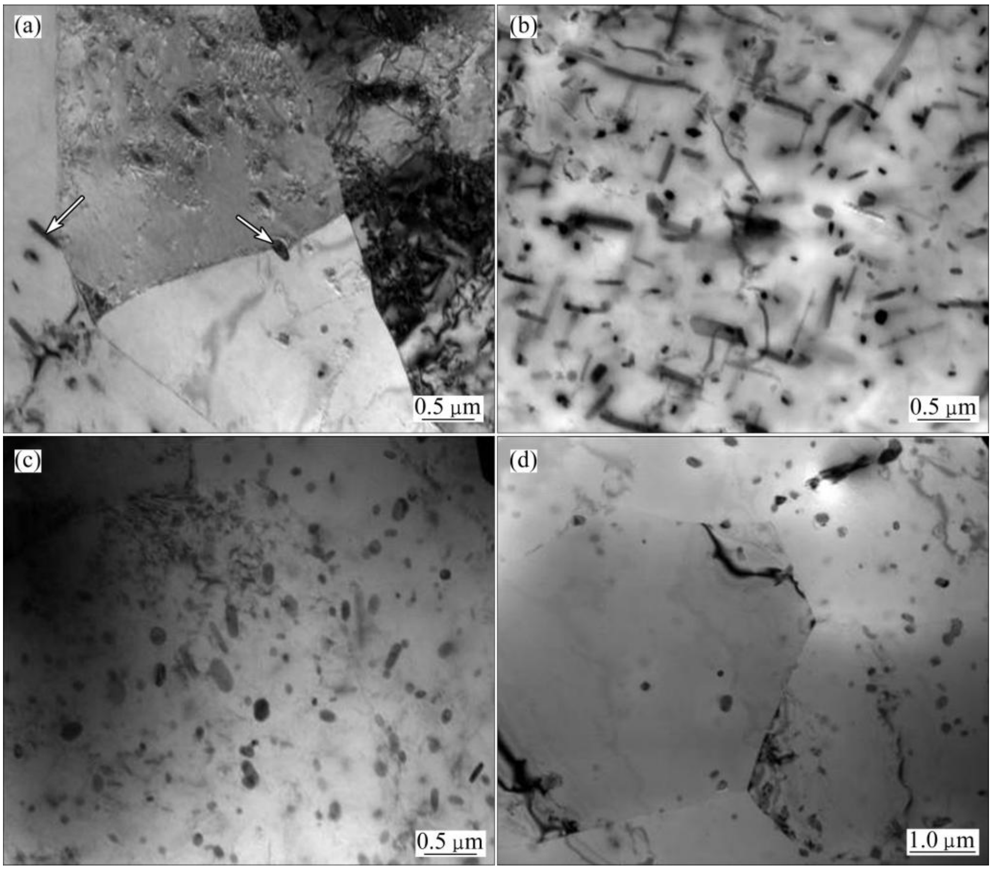

Fig. 7 TEM images showing morphological characters of precipitates: (a) 320 ℃, 0.01 s^{-1}, ln Z=61.3; (b) 320 ℃, 0.001 s^{-1}, ln Z=59.0; (c) 530 ℃, 10 s^{-1}, ln Z=51.0; (d) 530 ℃, 0.001 s^{-1}, ln Z=41.8

was no direct experimental evidence. The reason is ascribed to the growth of these particles by Ostwald ripening [34]. The coarse particles lead to a decrease in the pinning force on low-angle boundaries or dislocations. Consequently, the continuous flow softening is more likely to occur (Figs. 2(a) and (b)). As the deformation temperature increases to 530 ℃, which is close to the solvus temperature, the precipitates in the specimen deformed at 0.001 s^{-1} are much less and smaller than those in the specimen deformed at 10 s^{-1} (Figs. 7(c) and (d)). This can be attributed to the low strain rate, which allows more time for precipitates to dissolve into the matrix at 530 ℃ and 0.001 s^{-1}. The flow softening due to coarsening of dynamic precipitation is restricted. Therefore, the morphology and distribution of dynamic precipitates are important factors for flow softening during hot deformation.

4 Conclusions

1) The flow stress exhibits a continuous flow softening behavior at low deformation temperatures (≤390 ℃), whereas it reaches steady state at high temperatures (≥460 ℃). The high activation energy Q value (325.12 kJ/mol) of the alloy is related to the high Cu content in the alloy.

2) A linear relationship between recrystallized grain size (D_{rex}) and ln Z is established.

3) At high ln$Z$ values, prominent dynamic recrystallization and coarsening of dynamic precipitation may be responsible for the continuous flow softening behavior. With decreasing ln Z value, the second phase particles dissolve progressively into matrix during hot compression.

4) The microstructures of specimens with closer ln Z values are compared, dynamic recrystallization is more obvious in the specimen deformed at high temperature and strain rate (530 ℃, 10 s^{-1}) than that in the specimen deformed at low deformation temperature and strain rate (460 ℃, 0.1 s^{-1}).

References

[1] SHAH K B, KUMAR S, DWIVEDI D K. Aging temperature and abrasive wear behaviour of cast Al−(4%, 12%, 20%)Si−0.3%Mg alloys [J]. Materials and Design, 2007, 28: 1968−1974.

[2] SINGH R K, SINGH A K, ESWARA PRASAD N. Texture and mechanical property anisotropy in an Al−Mg−Si−Cu alloy [J]. Materials Science and Engineering A, 2000, 277: 114−122.

[3] ZHANG Hui, LI Luo-xing, YUAN Deng, PENG Da-shu. Hot deformation behavior of the new Al−Mg−Si−Cu aluminum alloy during compression at elevated temperatures [J]. Materials Characterization, 2007, 58: 168−173.

[4] MCQUEEN H J, BLUM W. Dynamic recovery: Sufficient mechanism in the hot deformation of Al (<99.99) [J]. Materials Science and Engineering A, 2000, 290: 95−107.

[5] GOURDET S, MONTHEILLET F. An experimental study of the recrystallization mechanism during hot deformation of aluminium [J]. Materials Science and Engineering A, 2000, 283: 274−288.

[6] KASSNER M E, BARRABESS R. New developments in geometric dynamic recrystallization [J]. Materials Science and Engineering A, 2005, 410−411: 152−155.

[7] DOHERTY R D, HUGHES D A, HUMPHREYS F J, JONAS J J, JUUL JENSEN D, KASSNER M E, KING W E, MCNELLEY T R, MCQUEEN H J, ROLLETT A D. Current issues in recrystallization: A review [J]. Materials Science and Engineering A, 1997, 238: 219−274.

[8] HOGG S C, PALMER I G, THOMAS L G, GRANT P S. Processing, microstructure and property aspects of a spray-cast Al−Mg−Li−Zr alloy [J]. Acta Materialia, 2007, 55: 1885−1894.

[9] ZHANG Zhi-ye, PAN Qing-lin, ZHOU Jian, LIU Xiao-yan, CHEN Qin. Hot deformation behavior and microstructural evolution of Al−Zn−Mg−0.25Sc−Zr alloy during compression at elevated temperatures [J]. Transactions of Nonferrous Metals Society of China, 2012, 22(7): 1556−1562.

[10] LIU Wen-yi, ZHAO Huan, LI Dan, ZHANG Zhi-qing, HUANG Guang-jie, LIU Qing. Hot deformation behavior of AA7085 aluminum alloy during isothermal compression at elevated temperature [J]. Materials Science and Engineering A, 2014, 596: 176−182.

[11] CHANG C S T, DUGGAN B J. Relationships between rolled grain shape, deformation bands, microstructures and recrystallization textures in Al−5%Mg [J]. Acta Materialia, 2010, 58: 476−489.

[12] BELADI H, CIZEK P, HODGSON P D. Texture and substructure characteristics of dynamic recrystallization in a Ni−30%Fe austenitic model alloy [J]. Scripta Materialia, 2009, 61: 528−531.

[13] WANG Xiao-feng, GUO Ming-xing, CAO Ling-yong, LUO Jin-ru, ZHANG Ji-shan, ZHUANG Lin-zhong. Influence of thermomechanical processing on microstructure, texture evolution and mechanical properties of Al−Mg−Si−Cu alloy sheets [J]. Transactions of Nonferrous Metals Society of China, 2015, 25(6): 1752−1762.

[14] LEE B H, REDDY N S, YEOM J T, LEE C S. Flow softening behavior during high temperature deformation of AZ31 Mg alloy [J]. Journal of Materials Processing Technology, 2007, 187−188: 766−769.

[15] BHATTACHARYA R, WYNNE B P, RAINFORTH W M. Flow softening behavior during dynamic recrystallization in Mg−3Al−1Zn magnesium alloy [J]. Scripta Materialia, 2012, 67: 277−280.

[16] LI Luo-xing, WANG Guan, LIU Jie, YAO Zai-qi. Flow softening behavior and microstructure evolution of Al−5Zn−2Mg aluminum alloy during dynamic recovery [J]. Transactions of Nonferrous Metals Society of China, 2014, 24(1): 42−48.

[17] QUAN Guo-zheng, LIU Ke-wei, ZHOU Jie, CHEN Bin. Dynamic softening behaviors of 7075 aluminum alloy [J]. Transactions of Nonferrous Metals Society of China, 2009, 19(S3): s537−s541.

[18] LIU Sheng-dan, YOU Jiang-hai, ZHANG Xin-ming, DENG Yun-lai, YUAN Yu-bao. Influence of cooling rate after homogenization on the flow behavior of aluminum alloy 7050 under hot compression [J]. Materials Science and Engineering A, 2010, 527: 1200−1205.

[19] WANG Ming-liang, JIN Pei-peng, WANG Jin-hui, HAN Li. Hot deformation behavior of as-quenched 7005 aluminum alloy [J]. Transactions of Nonferrous Metals Society of China, 2014, 24(9): 2796−2804.

[20] MIRZADEH H. Simple physically-based constitutive equations for hot deformation of 2024 and 7075 aluminum alloys [J]. Transactions of Nonferrous Metals Society of China, 2015, 25(5): 1614−1618.

[21] YANG Dong, QUAN Yong-hong, ZHAO Huan, ZHANG Zhi-qing, HUANG Guang-jie, LIU Qing. Effects of deformation heating on constitutive analysis of a new Al−Mg−Si−Cu alloy during hot

compression [J]. Materials Science Forum, 2014, 794−796: 1263−1268.

[22] SPIGARELLI S, EVANGELISTA E, MCQUEEN H J. Study of hot workability of a heat treated AA6082 aluminum alloy [J]. Scripta Materialia, 2003, 49: 179−183.

[23] HERBA E M, McQUEEN H J. Influence of particulate reinforcements on 6061 materials in extrusion modeling [J]. Materials Science and Engineering A, 2004, 372: 1−14.

[24] ZHANG B, BAKER T N. Effect of the heat treatment on the hot deformation behaviour of AA6082 alloy [J]. Journal of Materials Processing Technology, 2004, 153−154: 881−885.

[25] van HUIS M A, CHEN J H, SLUITER M H F, ZANDBERGEN H W. Phase stability and structural features of matrix-embedded hardening precipitates in Al−Mg−Si alloys in the early stages of evolution [J]. Acta Materialia, 2007, 55: 2183−2199.

[26] DING L P, JIA Z H, ZHANG Z Q, SANDERS R E, LIU Q, YANG G. The natural aging and precipitation hardening behaviour of Al−Mg−Si−Cu alloys with different Mg/Si ratios and Cu additions [J]. Materials Science and Engineering A, 2015, 627: 119−126.

[27] JIN Man, LI Jing, SHAO Guang-jie. The effects of Cu addition on the microstructure and thermal stability of an Al−Mg−Si alloy [J]. Journal of Alloys and Compounds, 2007, 437: 146−150.

[28] SHEN Y F, GUAN R G, ZHAO Z Y, MIARA R D K. Ultrafine-grained Al−0.2Sc−0.1Zr alloy: The mechanistic contribution of nano-sized precipitates on grain refinement during the novel process of accumulative continuous extrusion [J]. Acta Materialia, 2015, 100: 247−255.

[29] LIAO Heng-cheng, WU Yu-na, ZHOU Ke-xin, YANG Jian. Hot deformation behavior and processing map of Al−Si−Mg alloys containing different amount of silicon based on Gleebe−3500 hot compression simulation [J]. Materials and Design, 2015, 65: 1091−1099.

[30] DENG Ying, XU Guo-fu, YIN Zhi-min, LEI Xue-feng, HUANG Ji-wu. Effects of Sc and Zr microalloying additions on the recrystallization texture and mechanism of Al−Zn−Mg alloys [J]. Journal of Alloys and Compounds, 2013, 580: 412−426.

[31] ESMAEILI S, LLOYD D J. Effect of composition on clustering reactions in AlMgSi(Cu) alloys [J]. Scripta Materialia, 2004, 50: 155−158.

[32] JAZAERI H, HUMPHREYS F J. The transition from discontinuous to continuous recrystallization in some aluminium alloys II — Annealing behavior [J]. Acta Materialia, 2004, 52: 3251−3262.

[33] LI Jun-peng, SHEN Jian, YAN Xiao-dong, MAO Bai-ping, YAN Liang-ming. Microstructure evolution of 7050 aluminum alloy during hot deformation [J]. Transactions of Nonferrous Metals Society of China, 2010, 20(2): 189−194.

[34] LANG Yu-jing, CAI Yuan-hua, CUI Hua, ZHANG Ji-shan. Effect of strain-induced precipitation on the low angle grain boundary in AA7050 aluminum alloy [J]. Materials and Design, 2011, 32: 4241−4246.

高铜 6A82 铝合金在等温热压缩过程中的流变应力和显微组织演变

杨群英，杨 东，张志清，曹玲飞，吴晓东，黄光杰，刘 庆

重庆大学 材料科学与工程学院，重庆 400045

摘　要：在 Gleeble−1500 热模拟机上通过等温热压缩试验研究高铜 6A82 铝合金(Al−Mg−Si−Cu)在变形温度为 320~530 ℃、应变速率为 0.001~10 s^{-1} 条件下的流变应力和显微组织演变。结果表明，合金的流变应力在变形温度为 320~390 ℃ 的范围内呈连续软化行为，在温度高于 460 ℃ 的条件下达到稳定状态。合金的流变行为受双曲正弦形式的本构方程(Zener−Hollomon 参数 Z)影响，其热变形激活能为 325.12 kJ/mol。显微组织表征表明，明显的动态再结晶和动态析出的粗化导致流变应力的连续软化。在相近的 ln Z 值条件下，变形热使合金在 530 ℃、10 s^{-1} 条件下的动态再结晶比 460 ℃、0.1 s^{-1} 条件下的更加明显。

关键词：Al−Si−Mg−Cu 铝合金；等温热压缩；流变应力；动态再结晶；动态析出

(Edited by Wei-ping CHEN)